Electric-field-induced stretching of surface-tethered polyelectrolytes in a microchannel

Tamal Roy,[1,*] Kai Szuttor,[2] Jens Smiatek,[2] Christian Holm,[2] and Steffen Hardt[1]
[1]*Institute for Nano- and Microfluidics, Technische Universität Darmstadt, 64287 Darmstadt, Germany*
[2]*Institut für Computerphysik, Universität Stuttgart, 70569 Stuttgart, Germany*
(Received 5 June 2017; revised manuscript received 23 August 2017; published 27 September 2017)

We study the stretching of a surface-tethered polyelectrolyte confined between parallel surfaces under the application of a dc electric field. We explore the influence of the electric-field strength, the length of the polyelectrolyte, and the degree of confinement on the conformation of the polyelectrolyte by single-molecule experiments and coarse-grained coupled lattice-Boltzmann molecular-dynamics simulations. The fractional extension of the polyelectrolyte is found to be a universal function of the product of the applied electric field and the molecular contour length, which is explained by simple scaling arguments. The degree of confinement does not have any significant influence on the stretching. We also confirm that an electrohydrodynamic equivalence principle relating the stretching in an electric field to that in a flow field is applicable.

DOI: 10.1103/PhysRevE.96.032503

I. INTRODUCTION

Within the past three decades, exploring the behavior of polyelectrolytes under external forces has been an active area of research, extending from the comprehensive study of the conformations and physical properties of the macromolecules [1–12] to applications in the field of genomics [13–18]. The most convenient way to manipulate a polyelectrolyte is to expose it to an electric field [19–25]. This is particularly relevant in bioanalytical methods such as size-based electrophoretic separation (e.g., DNA and proteins) [26,27] or DNA sequencing by direct linear analysis [17,28]. In electrophoretic separation, the molecules migrate in response to the applied electric field and the migration velocity depends on the electrophoretic mobility of the molecule. Above a certain molecular size (e.g., double-stranded DNA of 400 base pairs), the electrophoretic mobility becomes size independent in bulk solution [29]. There are different techniques for separating larger molecules [17,28,30]. The most common among these is to use a sieving matrix (e.g., a cross-linked gel) to impose a size-dependent friction force on the molecules. Apart from the slab-gel electrophoresis setup, microfluidic devices have become popular recently for DNA size separation [31]. The gel-based separation using a constant electric field, however, does not work efficiently with DNA molecules larger than about 20 000 base pairs [32]. Therefore, elaborate techniques such as pulsed-field gel electrophoresis are required to achieve a size separation. An alternative technique to separate large DNA molecules is to attach one end of a DNA molecule to a solid surface, apply a dc electric field, and subsequently detach the molecules from the surface depending on their size [33,34]. These examples indicate that it is important to study the stretching of end-anchored polyelectrolytes in electric fields. Moreover, the recent advancement of microfabrication processes revolutionized bioanalytical protocols implemented in lab-on-a-chip devices [35,36]. Therefore, the behavior of polyelectrolytes in microfluidic devices has been an active field of research [37,38].

The stretching of polyelectrolytes under electric fields has been extensively studied in the past, based on experimental [3,5,39], numerical [2,6,7,10], and theoretical methods [9,40,41]. Double-stranded DNA molecules are often used as model polyelectrolytes because of their well-defined electrophoretic mobility, convenient fluorescence imaging, and excellent chemical modifiability. In the presence of counterions in the solution, a Debye layer forms around the charged backbone of the DNA molecules. The thickness of the Debye layer is given by

$$\lambda_D = \left(\frac{\epsilon_0 \epsilon_r k_B T}{e^2 \sum_i z_i^2 C_i} \right)^{1/2}, \tag{1}$$

where ϵ_0 is the vacuum permittivity, ϵ_r the dielectric constant of the solution, k_B the Boltzmann constant, T the absolute temperature, e the elementary charge, z_i the valance of the ith ionic species, and C_i the number density of the ith ionic species. In free-solution electrophoresis (i.e., in the absence of a sieving matrix) and in the presence of counterions, DNA molecules are free draining, i.e., no net force is exerted that deforms the chains. This is often explained by the absence of intrachain hydrodynamic interactions in the resulting electro-osmotic flow (EOF) around the charged backbone. For sufficiently thin Debye layers, each segment of a DNA molecule experiences the same hydrodynamic drag force and consequently the electrophoretic mobility of the molecule becomes size-independent [7,42].

The screening of hydrodynamic interactions in the EOF originating from the electric double layer around a polyelectrolyte chain is a prerequisite for the so-called electrohydrodynamic equivalence principle (EHEP) [40,43]. The EHEP states that the stretching of a tethered polyelectrolyte molecule in an electric field is the same as in the case when the tethered molecule is exposed to a uniform flow velocity $v = \mu E$, where μ is the electrophoretic mobility of the molecule and E is the electric field. As simple as it may appear, the scenario underlying the EHEP for a surface-tethered polyelectrolyte is quite subtle and it appears questionable if the EHEP can be applied to a broad class of problems. First, to ensure the screening of hydrodynamic interactions, the Debye length needs to be small enough. Second, a charged polyelectrolyte represents a localized source of EOF. The overall resulting flow field depends on the presence of boundaries such as channel

*roy@nmf.tu-darmstadt.de

walls and usually a pressure-driven flow field is created as a consequence of that if the localized source is fixed with respect to the boundaries. This means that even in the case of sufficiently thin Debye layers, hydrodynamic interactions between different parts of a polyelectrolyte chain may get reintroduced via the pressure-driven part of the flow field. The fact that a tethered polyelectrolyte in an electric field gets stretched at all is due to the pressure-driven flow that builds up as a reaction to the EOF around the charged backbone. Despite all of these limitations and subtleties, the EHEP has been confirmed experimentally [39]. To further explore its validity, it is worth probing the EHEP under different geometric constraints.

Polyelectrolytes tethered to a surface are the focus of the present study. Surface-tethered polymers stretched by external forces are relevant in a number of practical applications [17,34,44–46]. It is interesting to study the conformations and stretching of surface-tethered DNA molecules in the confinement of a microchannel, since such channels are often used in state-of-the art bioanalytical protocols. In this work we study the stretching of surface-tethered DNA molecules under a dc electric field both experimentally and by coarse-grained lattice-Boltzmann molecular-dynamics simulations. Molecules of different contour lengths are observed in microchannels of different heights smaller than the contour length of the molecule. In addition to that, we compare the stretching of DNA under an electric field to the stretching under pressure-driven flow.

II. EXPERIMENTAL DETAILS

A. Materials

SU-8 was purchased from Microchem and poly(dimethyl siloxane) (PDMS) from Dow Corning (Sylgard 184 silicone elastomer kit). Glass coverslips 170 μm thick were purchased from Menzel. λ-DNA and YOYO-1 intercalating dye were purchased from Invitrogen. The dNTP set, biotin-dUTP, Klenow exo$^-$, and T4 DNA ligase are from Thermo Scientific. (3-glycidyloxypropyl)trimethoxysilane (GPTMS), streptavidin, polyvinylpyrrolidone (PVP), and β-marcaptoethanol were purchased from Sigma-Aldrich.

B. Microchannel fabrication

We fabricated an SU-8 master structure using UV lithography. A PDMS monomer solution was mixed with cross-linkers (mixing ratio 10:1) and was degassed after thorough mixing. The degassed mixture was then poured onto the structured wafer and heated to 80 °C for 1 h to obtain a negative of the SU-8 master. The heights of the channel structures obtained in this way are 3.6, 6, 6.7, and 7.6 μm, respectively. The widths of the microchannels are 40–60 μm, and the length is 10 mm. Finally, we punched inlet and outlet holes and covered the channels with glass coverslips using oxygen plasma activation.

C. Surface modification of microchannels

We used the well-known biotin-streptavidin affinity to tether λ-DNA and concatemers of λ-DNA onto the channel surface. During the oxygen plasma activation process, hydroxyl groups are formed at the channel surface. The activated channel surface was then treated for 5 min with a solution of GPTMS (1 vol %) in 95% ethanol to create epoxy groups on the surface which enhance the streptavidin adsorption [47,48]. After that, the GPTMS solution was rinsed off and the channels were filled with 0.01-mg mL^{-1} aqueous streptavidin solution. Then the channels were kept at 4 °C overnight for streptavidin adsorption. Finally, the channels were rinsed with water to remove the unbound streptavidin.

D. DNA concatenation

λ-DNA molecules were concatenated, taking advantage of the complementary single-stranded overhangs at the ends of the molecules. We filled 1 μL of 0.33-μg μL^{-1} λ-DNA, 4 μL of 5X T4 DNA ligase buffer, and 1 μL of T4 DNA ligase (1 u μL^{-1}) into an Eppendorf tube and added autoclaved water to a total volume of 20 μL. The reagents were then mixed thoroughly and subsequently kept at room temperature for 25 min. Finally, the concatenated DNA molecules were separated from the reagents by ethanol precipitation.

E. End modification of DNA

After the concatenation, one end of the concatenated λ-DNA was selectively modified with biotin, taking advantage of the single-stranded overhangs at the end of the molecules. The base sequence of one of the overhangs is (ds-DNA)-TCCAGCGGCGGG-5′. The DNA solution was mixed with dATP, dGTP, biotin-dUTP, and the Klenow exo$^-$ fragment and left at 37 °C (ThermoMixer) for 20 min. After that the solution was heated at 70 °C to deactivate the enzyme and stop the reaction. The biotinylated DNA sample was then separated from unreacted nucleotides by ethanol precipitation. The separated and biotin-modified DNA sample was diluted with 0.5X TE (10 mM tris, 1 mM ethylenediaminetetraacetic acid, 10 mM NaCl, pH $\approx$ 8.0) buffer to a concentration of approximately 0.1 μg μL^{-1}. For visualization, the modified DNA molecules were mixed with the YOYO-1 intercalating dye (staining ratio 1:5) and subsequently diluted with 0.5X TE to obtain a final concentration of approximately 100 pg μL^{-1}. Then the sample containing biotin-modified concatemers of λ-DNA was introduced into the streptavidin-functionalized microchannels and left there for 10 min for tethering. Finally, the inlet and outlet reservoirs were emptied and subsequently filled with buffer solution (0.5X TE, 2% β-marcaptoethanol to prevent photobleaching), which is the medium flowing through the channels. Electro-osmotic flow in the microchannel was suppressed by adding 1% PVP to the DNA solution and the TE buffer.

F. Application of electric field

Platinum electrodes were placed in the inlet and outlet reservoirs. The electric field was applied using a QL355TP (Aim & Thurlby Thandar Instruments) dc power source. To eliminate any net flow in the channel, we connected one end of the channel to a pressure pump (Elveflow) controlled by a MATLAB graphical user interface and regulated the pressure inside the channel. A programmed voltage profile was defined using a MATLAB script that starts with a high output voltage

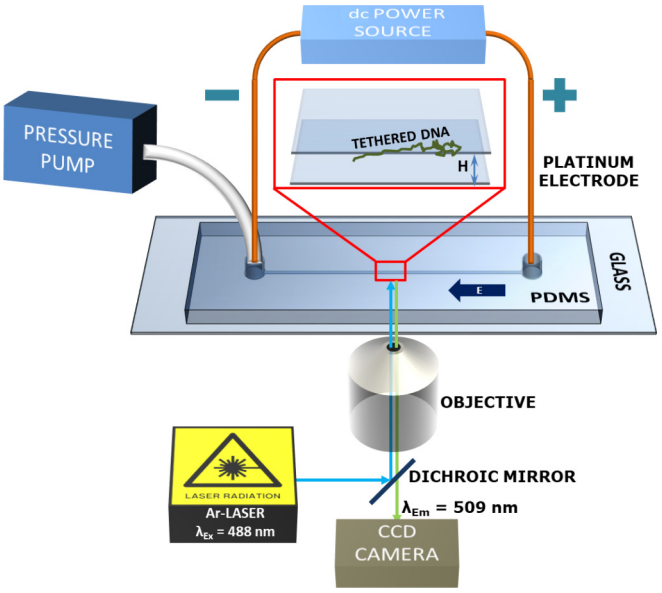

FIG. 1. Schematic diagram of the experimental setup.

(70 V across the channel) and reduces the voltage in steps of 5-s duration. This duration is significantly larger than the longest relaxation time of λ-DNA and the concatemers of λ-DNA [49]. Therefore, it is expected that the molecules attain a steady-state conformation during each step.

G. Visualization and image processing

The schematic diagram of the experimental setup is shown in Fig. 1. We used fluorescence microscopy to visualize single DNA molecules. A Nikon Eclipse Ti-E inverted laser scanning confocal microscope with a 100× oil-immersion objective (numerical aperture 1.49) was used to capture images of the DNA molecules in epifluorescence and confocal mode. The YOYO-1 intercalating dye was excited by an argon laser (488 nm) and the emitted signal (at 509 nm) was captured by an Andor iXon Ultra 897 CCD camera with 100-ms exposure time. The dynamics of the DNA molecules was recorded by epifluorescence microscopy. Fluctuations of the molecules normal to the tethering plane were captured by confocal microscopy. Capturing images in epifluorescence mode and confocal microscopy image processing was done using the NIS-Elements software. Confocal image stacks were captured using the EZ-C1 software. Image processing and data analysis was done by FreeStudio and MATLAB scripts.

III. SIMULATION DETAILS

We performed coarse-grained lattice-Boltzmann (LB) molecular-dynamics (MD) simulations with the simulation package ESPResSo [50,51]. The polymer is represented by a simple fully flexible bead-spring model with a purely repulsive shifted and cut Lennard-Jones potential [Weeks-Chandler-Andersen (WCA) potential [52]] according to

$$U_{\mathrm{WCA}}(r) = \begin{cases} 4\epsilon\left[\left(\frac{\sigma}{r}\right)^{12} - \left(\frac{\sigma}{r}\right)^{6}\right] + \epsilon & \text{for } r < 2^{1/6}\sigma \\ 0 & \text{otherwise,} \end{cases} \quad (2)$$

where σ is the diameter of a bead, r the distance between interacting beads, and $\epsilon = 1k_BT$ the energetic prefactor with the Boltzmann constant k_B and temperature T. Adjacent beads are connected by a finitely extensible nonlinear elastic bond potential

$$U_{\mathrm{FENE}}(r) = -\frac{1}{2}K\Delta r_{\mathrm{max}}^2 \ln\left[1 - \left(\frac{r - r_0}{\Delta r_{\mathrm{max}}}\right)^2\right], \quad (3)$$

with the spring constant $K = 30\epsilon/\sigma^2$, the maximum elongation $\Delta r_{\mathrm{max}} = 2.0\sigma$, and the minimum length $r_0 = 1.5\sigma$. The mass of a single bead is $m = m_0$. The number of beads varies in the simulations between $N = 30$ and $N = 90$. In addition to that, every bead bears a charge of $-1e$. A fixed excess number density of ions of $0.01\sigma^{-3}$ (equivalent to an excess salt concentration) is considered, which results in a Debye length of about 2σ. Electrostatic interactions are calculated by the particle-particle particle-mesh algorithm [53,54] with a correction for the two-dimensional periodicity of the channel geometry [55,56]. In order to include hydrodynamic interactions, we coupled the beads to a thermalized LB fluid [57,58]. The grid spacing of the LB fluid in a D3Q19 grid is $a = \sigma$. Furthermore, a mass density of $\rho = 1m_0/\sigma^3$ and a kinematic viscosity of $\nu_K = 1\sigma^2/\tau$ with the time scale $\tau = \sigma\sqrt{m_0/\epsilon}$ are used for the fluid properties. The coupling between the LB fluid and the MD beads is achieved by the standard scheme proposed by Ahlrichs and Dünweg [59] according to

$$\vec{F}_c = \Gamma(\vec{v}_m - \vec{u}), \quad (4)$$

where $\vec{F}_c$ is the coupling force on a bead, $\Gamma = 20m_0/\tau$ is the bare coupling constant, and $\vec{v}_m$ and $\vec{u}$ are the velocities of a bead and the fluid, respectively. The fluid velocity is calculated by a linear interpolation on the eight nearest neighbors. An equal and opposite force is applied to the fluid using the same weights used for the linear interpolation of the fluid velocity. For the lattice-Boltzmann simulations, the fluid and the coupling with the MD beads are thermalized using a lattice-Boltzmann thermostat such that $T = \epsilon = k_BT$. The time step for both the MD integration and the lattice-Boltzmann fluid is set to $\Delta t = 0.01\tau$. The physical boundaries of the microchannel are represented by two infinitely extended plates at $\pm z_B$ with a distance $H = 2z_B = 30\sigma$. The plates interact with the polymer beads via the same WCA potential as described above. A no-slip boundary condition at $\pm z_B$ is implemented via bounceback constraints on the LB grid [60]. We fixed the end bead at $-z_B$ in order to model a tethered polymer. The electric field is modeled by an external force (in the x direction) applied on each charged particle according to

$$\vec{F}_{\mathrm{x}} = q\vec{E}_{\mathrm{x}}, \quad (5)$$

where q denotes the charge of the respective particle and $\vec{E}_{\mathrm{x}}$ is the external electric field. We study the influence of external forces in the range between $0.01(\frac{1}{\sigma\tau^2})$ and $1.0(\frac{1}{\sigma\tau^2})$. A schematic illustration for our simulation setup is shown in Fig. 2.

IV. RESULTS AND DISCUSSION

Previous studies confirmed that the elasticity of a long DNA molecule is best described by the wormlike-chain

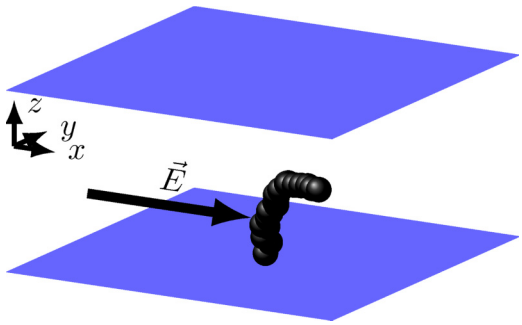

FIG. 2. Schematic drawing of a polymer (black spheres) tethered to a channel wall under the influence of an external electric field.

(WLC) model [61]. We make use of this fact to determine the contour lengths of the individual molecules employed in the experiments. The contour lengths are determined by fitting the extension vs electric-field data in the strongly stretched regime according to the WLC scaling relation $x/L \sim 1 - \xi E^{-1/2}$, where x is the extension of the molecules, L is the contour length, and ξ is a constant that depends on k_B, T, and the persistence length of the molecule. The extensions are normalized by the corresponding contour lengths to obtain fractional extensions. The validity of this method of determining the contour length was verified based on an alternative method where the increased contour length of a stained DNA molecule is estimated using the crystallographic data [62] and the staining ratio. The comparison of these two methods in terms of the scaling of the fractional extension with the applied electric-field strength in the strong-stretching regime is shown in Appendix A. Corresponding plots (Fig. 7 of Appendix A) indicate the validity of the WLC scaling in the strong-stretching regime.

Fluorescence microscopy images of a surface-tethered λ-DNA molecule at different values of the electric-field strength are shown in Fig. 3. Each image is a superposition of at least 18 consecutive images at the same value of the electric-field strength. In these images we notice that the lateral fluctuation (in a direction normal to the applied electric field) of the molecule is maximum at the free end and decreases continuously towards the tethered end. This can be attributed to the fact that, owing to the constant electric force per unit length of the chain, a nonuniform tension is created along the chain. The tension assumes its maximum value at the tethering point and decreases towards the end of the chain. An analytical

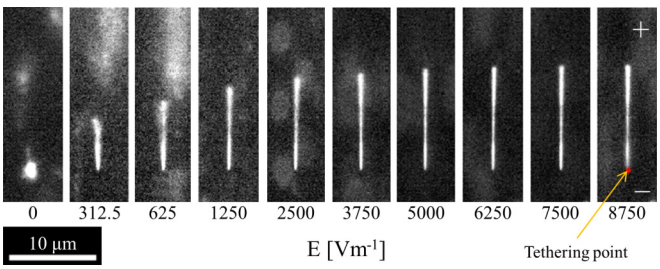

FIG. 3. Fluorescence microscopy images of a surface-tethered λ-DNA molecule in a 3.6-μm-deep channel. The contour length of the molecule is 20 μm.

expression based on this observation is derived in the next section.

A. Effect of contour length

We used λ-DNA, concatenated λ-DNA, and partially broken concatenated λ-DNA to obtain molecules of different contour lengths. For each set of contour lengths the extensions are determined by averaging the data of at least four different molecules. We captured the extension of DNA molecules with estimated average contour lengths of 14.6, 20.5, and 30.1 μm, respectively, under varying applied electric field in 3.6-μm-deep channels. We notice that, for a constant value of the electric field, the fractional extension increases with increasing contour length (plot not shown here). Qualitatively, this is expected because the stretching force on a molecule increases with the net effective charge (and hence the contour length) of the molecule. To explore the stretching in more detail, we plot the fractional extension as a function of EL in Fig. 4(a). We note that using EL as a scaling variable, the fractional extension curves for molecules of different contour lengths collapse onto a single curve. We performed similar experiments also in 6.7- and 7.6-μm-deep channels (data not shown here) and observed a result similar to that in 3.6-μm-deep channel, i.e., the fractional extensions collapse to a master curve if plotted against EL.

In the molecular-dynamics simulations, the contour length of the polyelectrolyte chain is directly proportional to the number of monomers N. In Fig. 4(b) the fractional extension of surface-tethered polyelectrolytes with $N = 30$–90 is plotted as a function of EN. We note that the fractional extensions collapse onto a master curve, indicating good agreement between the experimental and the MD simulation results.

The universality can be explained by the following arguments. A particular section of a tethered molecule experiences a stretching force exerted by its tail (i.e., the rest of the molecule towards the free end). We assume that at a particular position along the chain, the contour length associated with the tail is l. In general, the DNA molecules are exposed to an electric field and a nonelectric force. At a particular position along the chain, the nonelectric force is the stall force expressed as [40]

$$F_0(l) = \zeta(l)\mu E, \tag{6}$$

where $\zeta(l)$ is the drag coefficient of the tail length l and μ is the electrophoretic mobility of the molecule. In proximity to a solid surface, the intrachain hydrodynamic interaction is screened [63,64]. Qian *et al.* [65] showed that the diffusion coefficient D of a chain on a solid surface follows the Rouse scaling $D \sim L^{-1}$. By virtue of the fluctuation-dissipation theorem, the effective drag coefficient of a segment of length l is therefore proportional to l [i.e., $\zeta(l) \sim cl$], where c is a constant that depends on, among others, the viscosity of the buffer. Therefore, the electric force acting on the tail of the molecule of length l is

$$F_e(l) = F_0(l) = cl\mu E. \tag{7}$$

The extension of the chain segment located at a distance l (in terms of contour length) away from the free end of the molecule is due to the force $F_e(l)$. The extension of the complete chain can then be expressed as (similar to the method used by

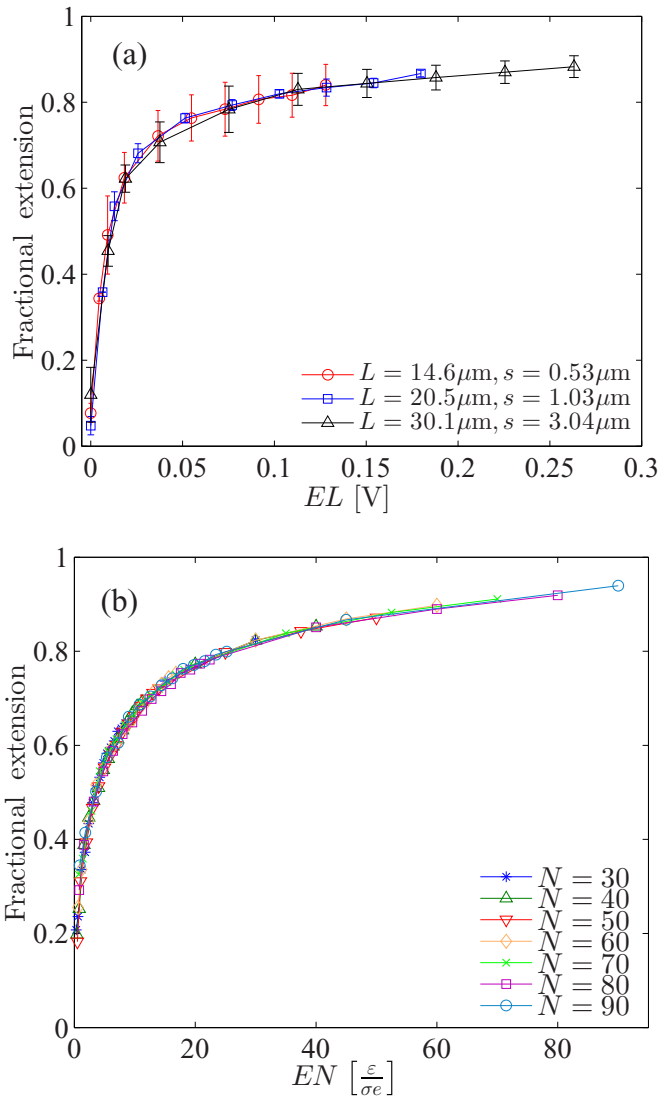

FIG. 4. Fractional extension plotted as a function of the product of the applied electric field and the respective molecular contour length. The lines are guides for the eye. (a) Extensions observed in experiments where L is the average contour length of four different molecules and s is the corresponding standard deviation of L. Error bars represent the standard deviation of the fractional extension. (b) Extensions observed in coupled LB-MD simulations.

Perkins *et al.* [66])

$$x = \int_{l=0}^{L} f^{-1}\left(\frac{F_e(l) l_p}{k_B T}\right) dl, \tag{8}$$

where l_p is the persistence length of the chain and f is a function describing the entropic elasticity of the chain as

$$F_s = f(z), \tag{9}$$

where F_s is the entropic spring force and $z = \frac{dx}{dl}$ is the fractional extension of the chain segment located at a distance l away from the free end of the molecule. We can express the tail length as $l = \alpha L$, where $0 < \alpha < 1$. With the help of Eq. (7), Eq. (8) can be rewritten as

$$\frac{x}{L} = \int_{\alpha=0}^{1} f^{-1}\left(\frac{c\alpha l_p \mu E L}{k_B T}\right) d\alpha. \tag{10}$$

Equation (10) clearly indicates that the fractional extension depends on E and L only via the combination EL. The expression on the right-hand side of Eq. (10) can be evaluated by numerical integration using an appropriate model of the chain elasticity. Corresponding plots of the fractional extension are included in Appendix B.

We note that the dependence of the fractional extension on the molecular contour length is different for a surface-tethered DNA molecule and the DNA molecules that are tethered away from a channel wall (see the work of Ferree and Blanch [39]). Ferree and Blanch found that the fractional extension is a universal function of $\mu E L^{0.54}$, whereas our results indicate that the fractional extension is a universal function of μEL. The difference in the scaling exponent of L can be attributed to the increase in the drag coefficient of the molecule near a solid surface compared to an unbounded flow [67].

B. Effect of channel height

To explore the effect of confinement, we studied the stretching of surface-tethered DNA molecules in microchannels with heights of 3.6, 6, 6.7, and 7.6 μm, respectively. Figure 5 shows the fractional extension of tethered λ-DNA molecules in these channels. The fractional extension curves do not show any clear trend with the channel height and, apart from deviations almost as small as the error bars, the extension curves are indistinguishable. We therefore conclude from Fig. 5(a) that the height of the channel does not significantly influence the extension of surface-tethered molecules stretched by a dc electric field under moderate confinement (i.e., $H < L$). This is expected, because we know from fluorescence microscopy that the DNA molecules stay quite close to the wall they are tethered to.

The degree of confinement depends not only on the height of the channel, but also on the size of the molecule. Therefore, an appropriate parameter that quantifies the confinement is $\frac{L}{H}$. An increase in this ratio indicates an increasing effect of confinement. The fractional extensions of the surface-tethered DNA molecules at the two extreme values of $\frac{L}{H}$ (=8.4 and 2.6) considered in this work are shown in Fig. 5(b). To eliminate the dependence on the molecular contour length (as discussed in Sec. IV A), the product of the applied electric-field strength and the respective molecular contour length is chosen as the independent variable. Figure 5(b) indicates a negligible influence of the confinement on the fractional extension of the tethered molecules.

C. Comparison between electric and hydrodynamic stretching

The EHEP relates the stretching of polyelectrolytes in an electric field to that due to a hydrodynamic flow. In our previous work [68], it was shown that a surface-tethered DNA molecule, when exposed to a pressure-driven flow inside a shallow channel, attains a strongly stretched conformation even at a small value of the wall shear rate (∼49 s^{-1}) and

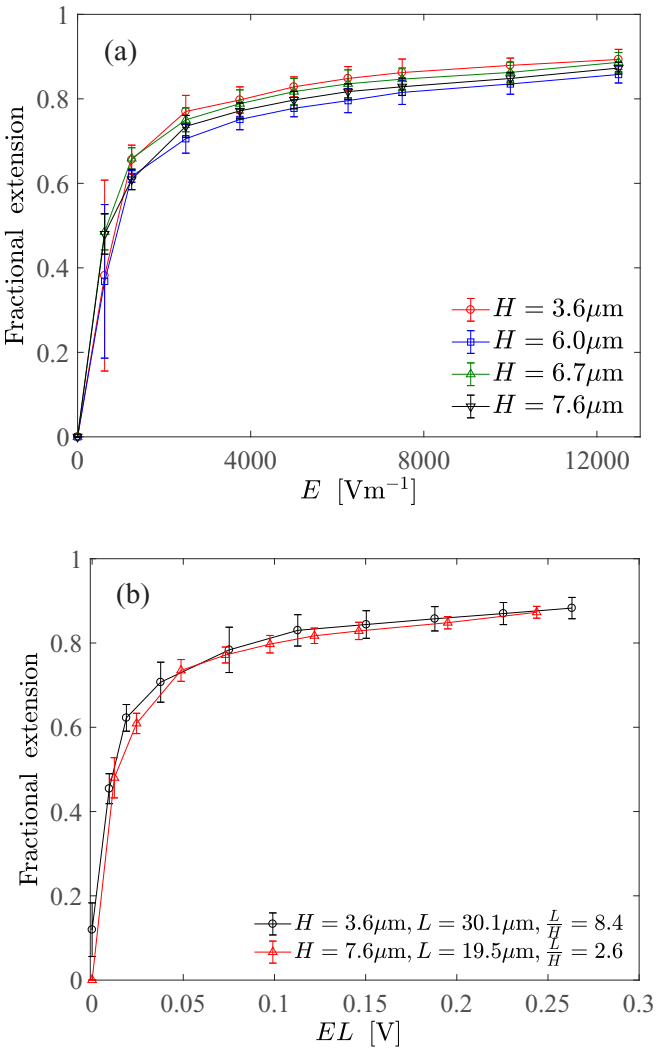

FIG. 5. (a) Fractional extension of tethered λ-DNA molecules plotted as a function of the applied electric field in channels of different heights. The error bars represent the standard deviation of the fractional extension. The lines are guides for the eye. (b) Fractional extension of tethered DNA molecules for the two extreme degrees of confinement considered in this work. The error bars represent the standard deviation. The lines are guides for the eye.

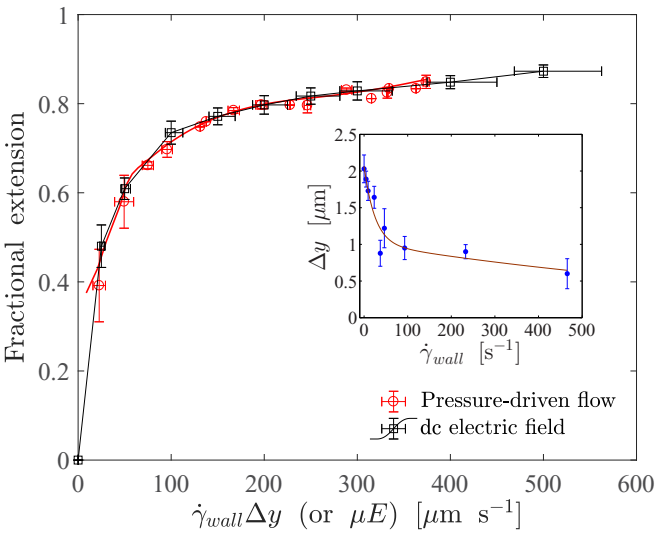

FIG. 6. Comparison of the stretching characteristics of surface-tethered λ-DNA in a 7.6-μm-deep microchannel under pressure-driven flow and under a dc electric field, respectively. The main diagram depicts the experimentally determined fractional extensions as a function of the equivalent force parameters, which are the product of the wall shear rate and the average distance from the wall for pressure-driven flow and the product of the electric field and the electrophoretic mobility for electric stretching. For the points corresponding to hydrodynamic stretching, the lines represent B-spline fits to the experimental data. For the points corresponding to electric stretching, the values are the average of the fractional extensions of seven different molecules and the error bars represent the corresponding standard deviation. The inset shows the average distance of the molecules from the wall as a function of the shear rate under pressure-driven flow.

remains close to the surface. According to a scaling argument given by Ladoux and Doyle [49], the transverse fluctuation of the tethered molecule diminishes as the molecule approaches the strong-stretching limit. The molecule therefore effectively experiences a flow profile with a constant shear rate. In the strong-stretching limit, the hydrodynamic drag force on a molecule can be approximated as

$$F_d \sim \zeta \dot{\gamma}_{\text{wall}} \Delta y, \tag{11}$$

where $\dot{\gamma}_{\text{wall}}$ is the shear rate at the wall and Δy is the average distance of the molecule from the tethering plane. Using this approximation, the EHEP states that molecules stretched by electric forces and hydrodynamic drag are expected to assume the same conformation if $\dot{\gamma}_{\text{wall}} \Delta y = \mu E$. We can therefore compare the fractional extensions of the molecules under the hydrodynamic drag force and under the electric field by plotting the corresponding fractional extensions as a function of $\dot{\gamma}_{\text{wall}} \Delta y$ and μE, respectively, in the same figure. We determined the average distance Δy of a λ-DNA from the tethering plane under pressure-driven flow by confocal microscopy. The inset plot in Fig. 6 shows the variation of the average distance of the molecules with the wall shear rate $\dot{\gamma}_{\text{wall}}$ in a 7.6-μm-deep microchannel. The experimental data were fitted with a curve consisting of two exponential functions. The fractional extension of λ-DNA is then plotted as a function of $\dot{\gamma}_{\text{wall}} \Delta y$, where the corresponding value Δy is obtained from the fitting curve. In the same figure, the fractional extension of electrically stretched λ-DNA molecules in the 7.6-μm-deep microchannel is plotted as a function of μE. We assume that $\mu = 4.0 \times 10^{-8}$ m^2 V^{-1} s^{-1}. This value represents the published experimental data for μ that range from 3.75×10^{-8} to 4.5×10^{-8} m^2 V^{-1} s^{-1} [29]. We note that the two fractional extension curves lie on top of each other, indicating that the EHEP is a useful concept for polyelectrolytes tethered to surfaces.

V. CONCLUSION

We studied the stretching of surface-tethered polyelectrolytes in a dc electric field under moderate confinement

(i.e., $H < L$). We used λ-DNA and concatemers of λ-DNA as model polyelectrolytes. The fractional extension is a universal function of the product of the applied electric-field strength and the molecular contour length, while no significant dependence on the channel height is found. The universal dependence on a scaling variable was explained based on a simple model. The experiments were supplemented by coarse-grained lattice-Boltzmann molecular-dynamics simulations using ESPResSo. Experimental and numerical simulation results are in good agreement. We also probed the electrohydrodynamic equivalence principle, relating the electric stretching of a polyelectrolyte to its stretching in a flow field. Good agreement between the two different stretching curves was found, indicating an equivalence between the conformations of surface-tethered polyelectrolytes under corresponding electric and hydrodynamic forces.

ACKNOWLEDGMENTS

We are grateful to Farough Roustaie, Institut für Elektromechanische Konstruktionen, Technische Universität Darmstadt, for the preparation of SU-8 master structures. We acknowledge financial assistance from the Deutsche Forschungsgemeinschaft (Grants No. HA 2696/33-1 and No. HO 1108/22-1).

APPENDIX A: VALIDITY OF WLC SCALING IN THE STRONGLY STRETCHED CONFORMATION

The elasticity of a double-stranded DNA molecule can be well described by the WLC model [49,61,69]. The scaling of the fractional extension of a WLC in the strong-stretching limit is given by [41]

$$\frac{x}{L} = 1 - \left(\frac{4Fl_p}{k_BT}\right)^{-1/2}, \tag{A1}$$

where x, L, and l_p are the extension, contour length, and persistence length of the chain, respectively, F is the deformation force acting on the chain, k_B is the Boltzmann constant, and T is the absolute temperature. To validate the scaling law for a surface-tethered DNA molecule, we estimated the contour length of a λ-DNA molecule from the staining ratio. The contour length of an unstained λ-DNA molecule (48 502 base pairs) is approximately 16.5 μm. In the experiments, the DNA molecules were intercalated with the YOYO-1 fluorescent dye, which untwists the double helix, resulting in an increase of the contour length of the molecules. According to crystallographic data [62], the contour length of a double-stranded DNA molecule increases by ∼4 Å per YOYO-1 molecule. We used a staining ratio of 1:5 (i.e., one YOYO-1 molecule per five base pairs). According to that, the contour length of a λ-DNA molecule is calculated as 20.4 μm.

Figure 7(a) shows the experimentally determined scaling of the fractional extension of λ-DNA molecules with the applied electric-field strength E, assuming the contour length $L = 20.4$ μm. The data indicate that the fractional extension of the tethered DNA molecules in the strong-stretching limit under the application of an electric field can be expressed by

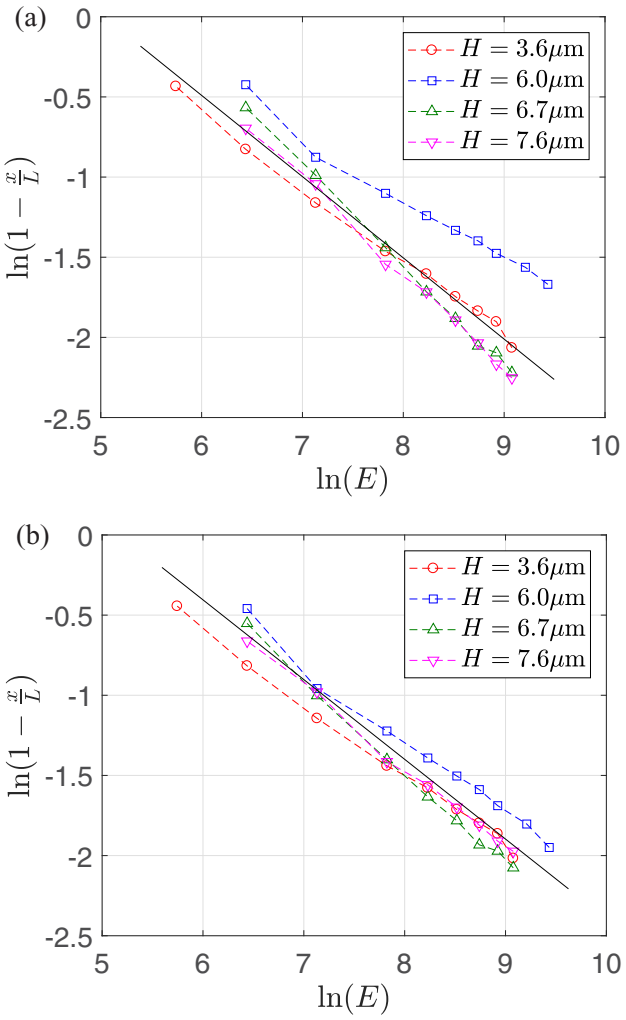

FIG. 7. (a) Scaling of $1 - \frac{x}{L}$ with E for λ-DNA assuming a constant contour length of 20.4 μm. The black solid straight line indicates a slope of $-\frac{1}{2}$. (b) Scaling of $1 - \frac{x}{L}$ with E for λ-DNA using the contour lengths determined from the WLC scaling in the strong-stretching limit. The black solid straight line indicates a slope of $-\frac{1}{2}$.

the WLC scaling, with a slight deviation for $H = 6.0$ μm. This deviation can be attributed to the statistical uncertainty in the degree of intercalation of the molecules. After having verified the validity of the WLC scaling in the strong-stretching limit at different degrees of confinement, we employ the scaling relationship to estimate the contour length of individual molecules more accurately. The variation of the fractional extension with the applied electric-field strength, based on the values of the contour length determined that way, is shown in Fig. 7(b).

APPENDIX B: RESULTS OF THE SCALING ANALYSIS

The extension of a surface-tethered chain under an electric field can be obtained from Eq. (8) by considering the local variation of the tension along the contour. The local fractional extension resulting from the local electric force $F_e(l)$

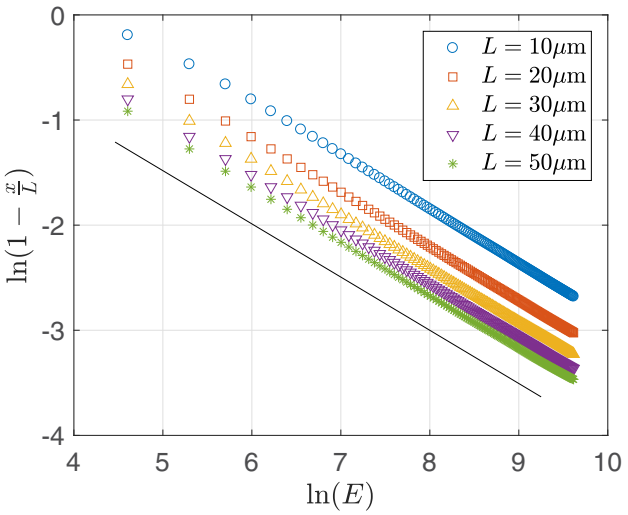

FIG. 8. Logarithm of the function appearing in the WLC scaling relation versus the logarithm of the electric-field strength. The black solid straight line indicates a slope of $-\frac{1}{2}$.

[i.e., the integrand in Eq. (8)] can be estimated from an appropriate model of the chain elasticity. The elasticity of a double-stranded DNA molecule can be described by the WLC model [49,61,69]. The corresponding elastic responses are different in the weak- and strong-stretching regimes. However, an effective interpolation formula for the WLC elasticity including the weak- and strong-stretching regimes was given by Marko and Siggia [41] as

$$f(z) = \frac{k_B T}{l_p}\left[z + \frac{1}{4(1-z)^2} - \frac{1}{4}\right], \tag{B1}$$

where z is the fractional extension and l_p is the persistence length of the chain. The expression on the right-hand side of Eq. (8) was evaluated using Eq. (B1). The corresponding numerical integration was performed using the trapezoidal rule. The plot shown in Fig. 8 confirms the validity of the WLC scaling considered in the main text when the local variation of the tension along the contour is taken into account.

[1] A. Erbas and M. Olvera de la Cruz, Macromolecules **49**, 9026 (2016).
[2] O. A. Hickey and C. Holm, J. Chem. Phys. **138**, 194905 (2013).
[3] C.-H. Lee and C.-C. Hsieh, Biomicrofluidics **7**, 014109 (2013).
[4] M. J. Stevens, D. B. McIntosh, and O. A. Saleh, Macromolecules **45**, 5757 (2012).
[5] J. Tang, N. Du, and P. S. Doyle, Proc. Natl. Acad. Sci. USA **108**, 16153 (2011).
[6] O. A. Hickey, C. Holm, J. L. Harden, and G. W. Slater, Phys. Rev. Lett. **105**, 148301 (2010).
[7] K. Grass and C. Holm, Soft Matter **5**, 2079 (2009).
[8] E. S. Shaqfeh, J. Non-Newtonian Fluid Mech. **130**, 1 (2005).
[9] A. E. Cohen, Phys. Rev. Lett. **91**, 235506 (2003).
[10] R. Netz, J. Phys. Chem. B **107**, 8208 (2003).
[11] N. C. Stellwagen, Colloids Surf. A **209**, 107 (2002).
[12] D. Stigter and C. Bustamante, Biophys. J. **75**, 1197 (1998).
[13] C. E. Gagna and W. C. Lambert, Pharmacogenomics **10**, 895 (2009).
[14] A. N. Rao and D. W. Grainger, Biomater. Sci. **2**, 436 (2014).
[15] D. Chatterjee, D. S. Mansfield, and A. T. Woolley, Anal. Meth. **6**, 8173 (2014).
[16] S. Laschi, R. Miranda-Castro, E. González-Fernández, I. Palchetti, F. Reymond, J. S. Rossier, and G. Marrazza, Electrophoresis **31**, 3727 (2010).
[17] E. Y. Chan, N. M. Goncalves, R. A. Haeusler, A. J. Hatch, J. W. Larson, A. M. Maletta, G. R. Yantz, E. D. Carstea, M. Fuchs, G. G. Wong, S. R. Gullans, and R. Gilmanshin, Genome Res. **14**, 1137 (2004).
[18] A.-D. Défontaines and J.-L. Viovy, Electrophoresis **14**, 8 (1993).
[19] K. K. Tetala and M. Vijayalakshmi, Anal. Chim. Acta **906**, 7 (2016).
[20] M. Li, W. Li, J. Zhang, G. Alici, and W. Wen, J. Phys. D **47**, 063001 (2014).
[21] T. Hahn and S. Hardt, Soft Matter **7**, 6320 (2011).
[22] T. Hahn and S. Hardt, Anal. Chem. **83**, 5476 (2011).
[23] R. E. Forster, D. G. Hert, T. N. Chiesl, C. P. Fredlake, and A. E. Barron, Electrophoresis **30**, 2014 (2009).
[24] J.-I. Won, Biotechnol. Bioprocess Eng. **11**, 179 (2006).
[25] C.-W. Kan, C. P. Fredlake, E. A. Doherty, and A. E. Barron, Electrophoresis **25**, 3564 (2004).
[26] R. K. Harstad, A. C. Johnson, M. M. Weisenberger, and M. T. Bowser, Anal. Chem. **88**, 299 (2015).
[27] E. Carrilho, Electrophoresis **21**, 55 (2000).
[28] E. Y. Chan, Mutat. Res.—Fundam. Mol. Mech. Mutagen. **573**, 13 (2005).
[29] N. C. Stellwagen, C. Gelfi, and P. G. Righetti, Biopolymers **42**, 687 (1997).
[30] G. H. Sanders and A. Manz, TRAC—Trends Anal. Chem. **19**, 364 (2000).
[31] G. Salieb-Beugelaar, K. Dorfman, A. Van den Berg, and J. Eijkel, Lab Chip **9**, 2508 (2009).
[32] B. Birren and E. Lai, *Pulsed Field Gel Electrophoresis: A Practical Guide* (Academic Press, New York, 2012).
[33] J. Wu, S.-L. Zhao, L. Gao, J. Wu, and D. Gao, Lab Chip **11**, 4036 (2011).
[34] L. Gao, J. Wu, D. Gao, and J. Wu, Appl. Phys. Lett. **91**, 113902 (2007).
[35] K. D. Dorfman, S. B. King, D. W. Olson, J. D. Thomas, and D. R. Tree, Chem. Rev. **113**, 2584 (2012).
[36] R. Marie and A. Kristensen, J. Biophoton. **5**, 673 (2012).
[37] S. Nedelcu and J.-U. Sommer, J. Chem. Phys. **133**, 244902 (2010).
[38] C.-C. Hsieh and P. S. Doyle, Korea-Aust. Rheol. J. **20**, 127 (2008).
[39] S. Ferree and H. W. Blanch, Biophys. J. **85**, 2539 (2003).
[40] D. Long, J.-L. Viovy, and A. Ajdari, Phys. Rev. Lett. **76**, 3858 (1996).
[41] J. F. Marko and E. D. Siggia, Macromolecules **28**, 8759 (1995).
[42] J.-L. Viovy, Rev. Mod. Phys. **72**, 813 (2000).

[43] D. Long, J.-L. Viovy, and A. Ajdari, Biopolymers **39**, 755 (1996).
[44] M. E. G. Lyons, in *Advances in Chemical Physics: Polymeric Systems*, edited by I. Prigogine and S. Rice (Wiley, New York, 1997).
[45] J. F. Joanny, Langmuir **8**, 989 (1992).
[46] S. Milner, Science **251**, 905 (1991).
[47] C. Mateo, V. Grazu, J. M. Palomo, F. Lopez-Gallego, R. Fernandez-Lafuente, and J. M. Guisan, Nat. Protoc. **2**, 1022 (2007).
[48] Q. Zhang, R. Huang, and L.-H. Guo, Chin. Sci. Bull. **54**, 2620 (2009).
[49] B. Ladoux and P. Doyle, Europhys. Lett. **52**, 511 (2000).
[50] H. J. Limbach, A. Arnold, B. A. Mann, and C. Holm, Comput. Phys. Commun. **174**, 704 (2006).
[51] A. Arnold, O. Lenz, S. Kesselheim, R. Weeber, F. Fahrenberger, D. Roehm, P. Košovan, and C. Holm, in *Meshfree Methods for Partial Differential Equations VI* (Springer, Berlin, Heidelberg, 2013), pp. 1–23.
[52] J. D. Weeks, D. Chandler, and H. C. Andersen, J. Chem. Phys. **54**, 5237 (1971).
[53] A. Arnold and C. Holm, in *Advanced Computer Simulation Approaches for Soft Matter Sciences II*, edited by C. Holm and K. Kremer, Advances in Polymer Sciences Vol. II (Springer, Berlin, Heidelberg, 2005), pp. 59–109.
[54] D. M. Heyes, J. Chem. Phys. **74**, 1924 (1981).
[55] A. Arnold, J. de Joannis, and C. Holm, J. Chem. Phys. **117**, 2496 (2002).
[56] A. Arnold, J. de Joannis, and C. Holm, J. Chem. Phys. **117**, 2503 (2002).
[57] B. Dünweg and A. J. C. Ladd, in *Advanced Computer Simulation Approaches for Soft Matter Sciences Vol. III*, edited by C. Holm and K. Kremer, Advances in Polymer Science (Springer, Berlin, Heidelberg, 2009), Vol. 221, pp. 89–166.
[58] D. Roehm and A. Arnold, Eur. Phys. J.: Spec. Top. **210**, 89 (2012).
[59] P. Ahlrichs and B. Dünweg, Int. J. Mod. Phys. C **9**, 1429 (1998).
[60] O. A. Hickey, C. Holm, and J. Smiatek, J. Chem. Phys. **140**, 164904 (2014).
[61] C. Bustamante, J. Marko, E. Siggia, and S. Smith, Science **265**, 1599 (1994).
[62] F. Johansen and J. P. Jacobsen, J. Biomol. Struct. Dyn. **16**, 205 (1998).
[63] O. B. Bakajin, T. A. J. Duke, C. F. Chou, S. S. Chan, R. H. Austin, and E. C. Cox, Phys. Rev. Lett. **80**, 2737 (1998).
[64] D. Long and A. Ajdari, Eur. Phys. J. E **4**, 29 (2001).
[65] H.-J. Qian, L.-J. Chen, Z.-Y. Lu, and Z.-S. Li, Phys. Rev. Lett. **99**, 068301 (2007).
[66] T. T. Perkins, D. E. Smith, R. G. Larson, and S. Chu, Science **268**, 83 (1995).
[67] J. Happel and H. Brenner, *Low Reynolds Number Hydrodynamics: With Special Applications to Particulate Media* (Springer Science + Business Media, New York, 2012), Vol. 1.
[68] T. Roy, K. Szuttor, J. Smiatek, C. Holm, and S. Hardt, Soft Matter (2017), doi: 10.1039/C7SM00306D.
[69] S. B. Smith, L. Finzi, and C. Bustamante, Science **258**, 1122 (1992).